JOURNAL OF SPACECRAFT AND ROCKETS
Vol. 30, No. 6, November–December 1993

Visible Spectra of Thruster Plumes from the Space Shuttle Primary Reaction Control System

Rodney A. Viereck*
Phillips Laboratory, Hanscom Air Force Base, Massachusetts 01731
Lawrence S. Bernstein†
Spectral Sciences Incorporated, Burlington, Massachusetts 01803
Stephen B. Mende‡
Lockheed Palo Alto Research Laboratory, Palo Alto, California 94304
Edmond Murad*
Phillips Laboratory, Hanscom Air Force Base, Massachusetts 01731
Gary R. Swenson‡
Lockheed Palo Alto Research Laboratory, Palo Alto, California 94304
and
Charles P. Pike§
Phillips Laboratory, Hanscom Air Force Base, Massachusetts 01731

In situ measurements of plume spectra from high-altitude, 870-lb, liquid propellent engine plumes have been obtained from observations of the Space Shuttle's primary reaction control system engines. Spectra were taken in the wavelength range of 350–800 nm with a spectral resolution of 3 nm and a spatial resolution of 10 cm. These spectra show numerous emissions from molecular and atomic species. There is significant variation in the spatial distribution of the emitting species. A survey of the auroral photography experiment (APE) thruster emission data will be given. The data will be compared to a chemical kinetic multizone flowfield model. This model was developed to analyze data from vacuum chamber tests. It incorporates 149 separate reactions and 53 distinct ground and excited state species, but this model is only valid around the exit plane of the thruster. A simplified exhaust plume model, valid for the first few meters of the plume, was then applied to the exit-plane conditions and the results are consistent with all of the major features of the data.

Introduction

IN an attempt to identify the sources of optical radiation generated by the interaction of the atmosphere with the exhaust from the Shuttle engines,[1] we report here spectroscopic observations of optical radiation near the exit of the nozzle of the primary reaction control system (PRCS) engines of the Space Shuttle. Spectra of the vacuum core (within 3 m of nozzle) of the Space Shuttle PRCS engines were taken as part of an experiment called the auroral photography experiment (APE).[2] The PRCS engines are liquid propellant motors and have a thrust of 870 lb. They are fueled by monomethylhydrazine (MMH) with N_2O_4 as an oxidizer. The near exit-plane emissions of this motor have been previously studied in a vacuum chamber.[3] There are many similarities between the vacuum chamber measurements and those presented here. The differences, however, are also striking. The space-based measurements extend from about 0.5 m from the exit plane to a distance of 3 m downstream in the plume thus covering a region of the plume never observed for an engine of this size either in space or in a vacuum chamber.

The PRCS motor is heavily film cooled with 25% of the fuel diverted to the outer walls of the combustion chamber for this purpose. As a result the chemical composition of the nozzle and exhaust plume flows can be broadly characterized by three distinct regions: 1) an outer fuel-rich zone due to the large quantity of fuel sprayed onto the combustor walls, 2) an inner oxidizer-rich zone due to the diversion of fuel to the outer walls, and 3) a mixing layer along the interface of the inner and outer zones. Previous analysis indicated that the OH, CO_2, and NO_2 radiation arise from recombination reactions such as $NO + O \rightarrow NO_2 + h\nu$, in the inner oxidizer-rich zone.[4] Fuel-rich flows can form energetic reactive fuel fragments, such as CH_2, C_2H_2, CH, C_2, C_2O, and others, by a combination of pyrolysis and oxidation chemistry. These species can then undergo very exothermic, one-step reactions with plume oxidizing species, such as O, NO, OH, and O_2, to produce electronically excited reaction products. All of the other emission features were found to arise from chemical reactions occurring in the mixing layer.

The data were obtained with a hand-held spectrograph operated by the astronauts from the aft flight deck of the Space Shuttle as part of the APE. The instrument recorded the spectrum between

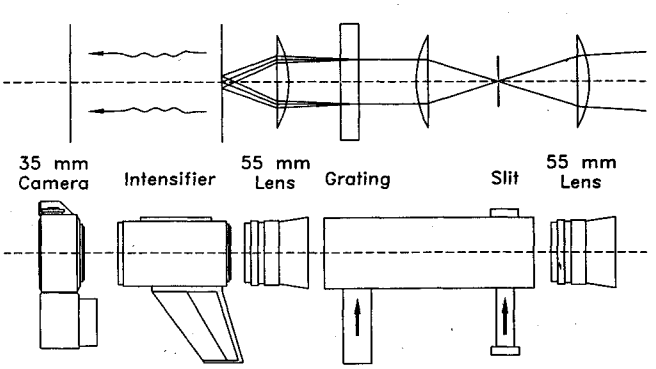

Fig. 1 APE spectrograph consisting of a slit, a diffraction grating, three lenses, an intensifier, and a 35-mm camera.

Received June 7, 1992; revision received Dec. 29, 1992; accepted for publication Jan. 6, 1993. This paper is declared a work of the U.S. Government and is not subject to copyright protection in the United States.

*Scientist, Spacecraft Interactions Branch.
†Scientist.
‡Research Scientist.
§Chief, Spacecraft Interactions Branch.

375 and 820 nm with a resolution of 3.5–4.0 nm on a two-dimensional detector. This provided spatial information parallel to the spectrograph slit. In the data presented here, the slit was parallel to the plume axis resulting in spatial measurement to a distance of 300 cm with a resolution of about 10 cm. The data were obtained from a series of 4-s PRCS thruster firings at an orbit altitude of 240 km. At this altitude the ambient atmosphere consists primarily of O atoms and the atmospheric pressure is of the order 2×10^{-8} Torr; however, the local pressure around the Shuttle can be as high as 10^{-6} Torr due to outgassing from the Shuttle surfaces.

The analysis presented here uses as its starting point the results from the chamber measurements[4] obtained using a coupled chemical-kinetic multizone flowfield model. The chemical-kinetic mechanism was motivated by the striking similarities in the UV-visible emission spectra from laboratory measurements of hydrocarbon flames[5–7] and conventional liquid propellant motors containing carbon fuels MMH and unsymmetrical dimethylhydrazine. It incorporates 149 separate reactions and 53 distinct ground and excited state species. The model is currently limited to the exit plane and is not yet applicable to the 3-m distance region sampled in the data set presented here. A simplified exhaust plume model is used to extend the calculations into the first few meters of the plume. The results are consistent with all of the major features of the data.

Experiment

The data were obtained with a hand-held spectrograph consisting of a 50-mm camera lens, a slit, a collimating lens, a transmissive diffraction grating, and a second 50-mm camera lens to refocus the spectra on to an intensifier. The spectrographic images were recorded with a Nikon 35-mm camera fitted with a battery powered, Noctron image intensifier with an S-20 photocathode. Figure 1 is a schematic drawing of the APE spectrograph. The spectrograph was operated from the aft flight deck of the Space Shuttle. Table 1 lists the parameters of the spectrograph system.

The APE spectrograph was flown on STS-38 in November 1990. The spectrograph was inside the Shuttle crew compartment on a bracket attached to the overhead window such that the instrument could observe the tail of the Orbiter through the aft flight-deck windows. The mounting device made it possible to point the spectrograph at a target and then lock it into position. The grating and slits were removable so the astronauts could observe an image of the target through the instrument and thus align the spectrograph slit on the target, parallel to the thruster axis. This orientation allowed us to measure variations in the plume spectra along the slit as a function of distance from the thruster nozzle.

Table 1 Parameters of the APE spectrograph and intensified camera

Lenses (2)	50 mm, f-1.2 (NASA provided hardware)
Wide slit	25×0.1 mm, 3-nm resolution
Narrow slit	25×0.03 mm, 1.1-nm resolution
Grating	600 lines/mm, blazed at −500 nm
Intensifier	S-20. 25-mm photocathode
Camera	Nikon 35 mm (NASA provided hardware)
Film	1600 ASA, Kodak Ektapress, color negative

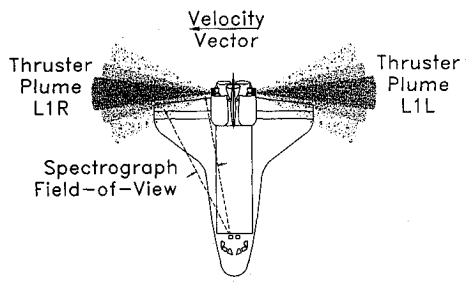

Fig. 2 Diagram of the Shuttle showing location and direction of the thrusters and the field of view of the APE spectrograph.

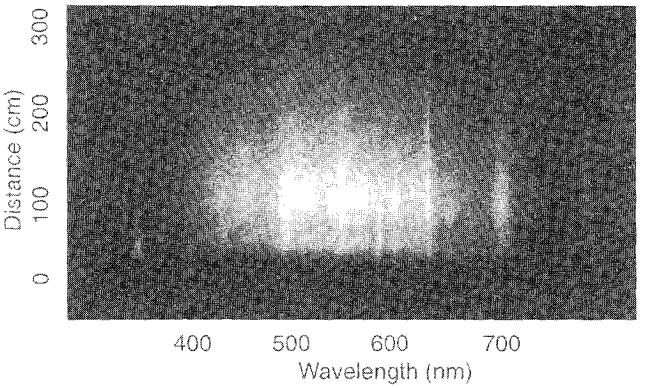

Fig. 3 Image of data showing spectral dispersion along the *X* axis and spatial dispersion along the *Y* axis.

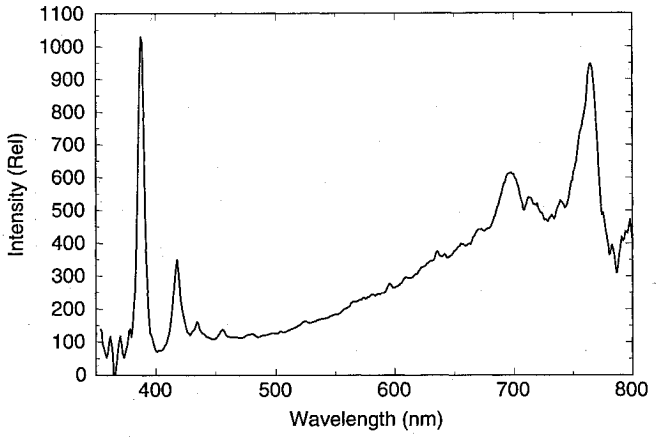

Fig. 4 Spectrum of the thruster plume about 100 cm from the exit plane of the thruster.

The Shuttle was near the equator at an altitude of 240 km and was placed in an orbital attitude with the right wing into the ram and the Shuttle bay toward the Earth. The thrusters that were fired were the L1L and R1R thrusters. These thrusters fire outward from behind the orbital maneuvering system pod. Figure 2 shows the location and direction of the thrusters that were fired and the location of the APE spectrograph on the aft flight deck of the Orbiter. The data were taken while the Orbiter was in darkness so that the primary luminance came from Shuttle thruster plume and from Earth airglow.

There were two slits available (see Table 1) providing two spectral dispersions. The wide slit (0.1 mm) allowed more light through to the detector but resulted in a spectral resolution of 3–4 nm. The narrow slit (0.03 mm) resulted in 1.5–2-nm resolution but allowed only one-third of the light of the wide slit through to the detector. For these measurements, the wide slit was used to guarantee adequate sensitivity. Future measurements will be taken with the narrow slit for additional spectral resolution.

For accurate wavelength calibration, spectra of the Earth-limb airglow were taken. The atomic oxygen lines at 557.7, 630.0, and 636.4 nm provided confirmation of the wavelength scale and the spectral resolution. The airglow measurements also provided confirmation of the spectral sensitivity calibration. The observed OH Meinel band variations could be compared to the known band intensities, thereby confirming the calibration of the system including the Orbiter window.

Data Reduction and Analysis

The color negative film was developed at NASA's photography laboratory and the processed film was digitized using a slide scanning system to produce image files in a format accessible by com-

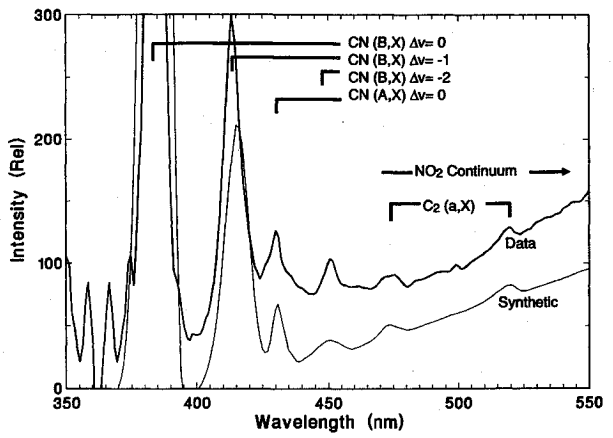

Fig. 5 Blue region of the spectrum shown in Fig. 4 (top curve) along with a synthetic spectrum (bottom curve) of CH, CN, C_2, and a laboratory spectrum of NO_2.

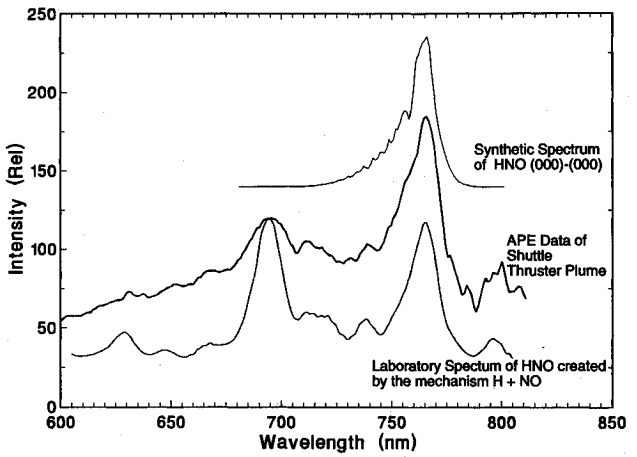

Fig. 6 Red region of the spectrum shown in Fig. 4 (middle curve) plotted with the laboratory spectrum of Ishiwata et al.[10] (bottom curve) and a synthetic spectrum of the (000)-(000) band at 800 K of HNO as calculated by Dressler.[13]

puters. The resulting images had dimensions of 512 × 350 pixels with 256 brightness levels. The response of film to light is nonlinear and thus a correction was determined from the preflight calibration data and then applied to the Shuttle data. Atomic oxygen emission lines at 557.7, 630.0, and 636.4 nm were present in the thruster data providing a check on the wavelength calibration of the data.

A spectrographic image of the thruster plume is shown in Fig. 3. The x axis is wavelength, the y axis is distance from the exit plane of the nozzle, and the various shades represent the brightness of the emission at a particular wavelength and distance from the exit plane. Note the bands near 400 nm and those near 700 nm. The bands in the red region of the spectrum extend further from the exit plane than do those in the blue.

Instrument sensitivity as a function of wavelength was determined by preflight and postflight calibration where the instrument was exposed to a continuum source of known brightness, and the resulting spectrum provided a measure of the instrument sensitivity. It should be noted that the Shuttle window could not be included in the preflight and postflight calibrations. Data taken on similar windows show about 80% transmission from 400 to 800 nm and < 1% transmission to the red and blue of this region. Details of the transition regions near 400 and 800 nm have not been provided and we have not been able to measure the window transmission function at the time of publication of this report.

The window transmission function from 640 to 820 nm was determined by applying a correction to the airglow data so that the OH Meinel bands, including the (6,1), (7,2), (8,3), (9,4), (4,0), and (5,1) bands, were in better agreement with the known vibrational distribution in the airglow. The details of the instrument calibration and window correction have been described in detail elsewhere.[8] The resulting correction was determined to be a decrease in transmission from 80% at 700 nm to about 20% at 830 nm. Figure 4 shows a corrected and calibrated spectrum of the PRCS thruster plume about 50 cm from the exit plane.

Numerous spectral features have been identified in the plume spectrum. The region between 350 and 600 nm has been expanded and compared to synthetic spectra as shown in Fig. 5. The spectral features in this figure, including CN(B →X), CH(A →X), and C_2(A →X) bands and NO_2 (Ref. 9) have been identified in previous plume spectra. The CN(B →X) bands are identifiable to $\Delta v = -2$. Also evident in the spectrum is a continuum emission presumably arising from NO_2. This emission rises from 400 nm and peaks near 700 nm and decreases again to the red of 700 nm. The instrument sensitivity decreases significantly below 380 nm and the transmission of the Shuttle window falls to near zero at about 370 nm, so neither the NH(A →X) bands at 336 nm nor the CN(B →X) $\Delta v = 1$ band at 360 nm are evident in the data. The decrease in instrument sensitivity and the resulting decrease in the signal-to-noise ratio is evident near the left edge of the image in Fig. 3.

One of the more prominent features, and one that has not typically been associated with rocket and Shuttle motors, is the emission between 650 and 800 nm identified as HNO. The spectrum between 550 and 800 nm is shown in Fig. 6 where laboratory spectra of HNO (Ref. 10) are compared to the data along with a synthetic spectrum of the (000)-(000) band of HNO at 800 K. The laboratory HNO spectrum is very similar in structure to the data presented here; however, the vibrational distribution of several of the bands is not in agreement. A synthetic spectrum of the ground state was calculated, and the result is shown in Fig. 6 along with the laboratory spectrum[10] and the data from this report. Spectral lines from two atomic species have been identified. The sodium emission at 589 nm was evident in the first meter of the plume. The atomic oxygen lines at 557.7 and 630.0 nm associated with the O^1S and O^1D states, respectively, were observed to extend beyond the instrument field of view. The $O(^1D)$ lines have also been identified in the far plume (0.25–2 km),[11] however, the excitation mechanism is presumed to be different in the vacuum core.

It should be noted that the HNO bands observed in the plume have different distributions than those observed in the laboratory. There is the possibility that emissions from other species such as the $O_2(^1\Sigma)$ 0-0 band may be present; however, the various excitation methods explored in the laboratory[11] produced very different HNO band ratios, implying that perfect agreement between the plume data and the laboratory data may not exist. Furthermore, the spatial distribution in the thruster plume of the HNO band at 765

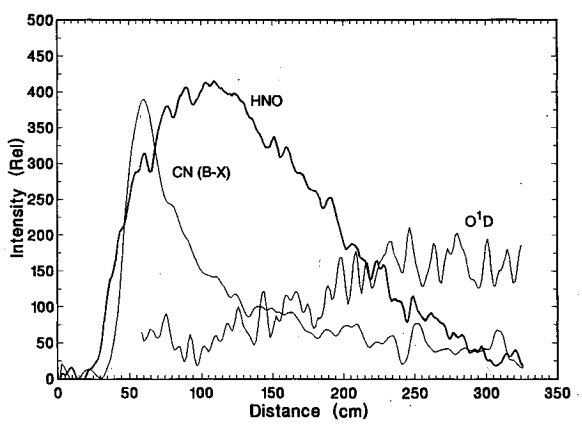

Fig. 7 Brightness of CN, HNO, and O plotted as functions of distance from the exit plane of the thruster nozzle.

nm is the same as for the band at 690 nm which is inconsistent with the O_2 theory. Also, the shape of the HNO (000)-(000) band observed in the thruster plume is very similar to both the synthetic and laboratory spectra and not similar to O_2 bands which have a trailing P branch to the red of the R branch. Finally, there is little evidence of any other O_2 bands such as the (1-1) and (2-2) bands. If O_2 emissions are present in the plume, they appear to have a minor contribution as compared to the HNO emission.

Examination of the spatial extent of the emissions provides some key insight as to the chemistry involved. The CH, CN, and C_2 emissions are observable only near the exit plane and become too weak to be observed downstream. This is shown in Fig. 7 where the spatial extent of CN, HNO, and O_2 are plotted. It should be noted that spatially, CH and C_2 are similar to CN. Likewise, the spatial distribution of NO_2 is similar to HNO. The NO_2 and HNO spectra actually increase in brightness out to about 100 cm where they too begin to decrease in brightness. The O^1D emission increases in intensity with increasing distance from the exit plane of the nozzle. The model calculations do not include a mechanism to create $O(^1D)$, however, for the extended plume, two processes have been proposed.[11]

In summary, we have identified molecular emissions arising from CN, CH, C_2, NO_2, and HNO and atomic emissions from O and Na. Spatially the CN, CH, C_2, and Na emissions are observed only within 1 m of the exit plane of the thruster nozzle. The remaining emissions from NO_2, HNO, and O extend several meters from the exit plane. The atomic oxygen emission increases in brightness with increasing distance from the exit plane.

Model Calculations

Two steps were required to calculate the downstream features (0–300 cm from the exit plane) of the thruster plumes. The first step was to use a chemical kinetic multizone flowfield model that incorporates 149 separate reactions and 53 distinct ground and excited state species but is only valid around the exit plane of the thruster. The exit-plane conditions calculated by this kinetic model are listed in Table 2.

Table 2 Summary of estimated PRCS exit-plane properties

Species	Mole fractions	
	Inner oxider-rich zone	Mixing layer
H	0.027	0.027
H_2	0.046	0.046
O	0.0028	0.0006
OH	0.0044	0.0022
NO	0.013	0.013
C_2H_2	0.0	5×10^{-5}
Oxider fuel	N_2O_4/MMH	
Overall oxidizer/fuel ratio	1.70	
Inner-zone oxidizer/fuel ratio	2.27	
Diameter D_e, cm	24.0	
Temperature T_e, K	1348	
Velocity V_e, m/s	2947	
Specific heat ratio, γ	1.26	
Density n_e, cm^{-3}	2.4×10^{17}	

Table 3 Key reactions and rate constants

	Reaction	Rate constant, cm^3/s
R1	$C_2H_2 + H \rightarrow C_2H + H_2$	$1.0\times10^{-5}T^{-1.38}\exp(-6350/T)$
R2	$C_2H + H_2 \rightarrow C_2H_2 + H$	$2.50\times10^{-11}\exp(-1555/T)$
R3	$C_2H + H \rightarrow C_2 + H_2$	$1.0\times10^{-10}\exp(-14{,}500/T)$
R4	$C_2H + OH \rightarrow C_2 + H_2O$	$1.0\times10^{-10}\exp(-9000/T)$
R5	$C_2H + C_2H \rightarrow C_2 + C_2H_2$	3.0×10^{-12}
R6	$C_2H + O \rightarrow CH + CO$	8.3×10^{-11}
R7	$C_2 + NO \rightarrow CN(B) + CO$	1.0×10^{-11}
R8	$CN(B) + M \rightarrow CN + M$	2.0×10^{-10}
R9	$CN(B) \rightarrow CN + h\nu$	1.5×10^{7} [a]
R10	$C_2 + NO \rightarrow CN(A) + CO$	7.0×10^{-10}
R11	$CN(A) + M \rightarrow CN + M$	2.0×10^{-10}
R12	$CN(A) \rightarrow CN + h\nu$	1.7×10^{5} [a]
R13	$O + NO \rightarrow NO_2 + h\nu$	$5.8\times10^{-17}(300/T)^2$
R14	$H + NO \rightarrow HNO + h\nu$	$4.6\times10^{-19}(300/T)^2$

[a]Einstein A coefficient, s^{-1}.

The second part of the calculations was to extend the chemical model several meters into the plume. To predict absolute emission intensities downstream of the exit plane, a simplified description of the flowfield properties of temperature and density was employed. The exhaust plume properties are assumed to depend only on axial distance from the exit (i.e., a top hot radial distribution) and are computed from the following relations for an isentropic flow:

$$n = \left[\frac{De}{(D_e + z)}\right]^2 n_e \tag{1}$$

and

$$T = \left[\frac{D_e}{(D_e + z)}\right]^{2(\gamma-1)} T_e \tag{2}$$

where n is number density in molecules/cubic centimeters, D_e the exit-plane diameter in centimeters, z the axial distance along the centerline in centimeters, T the temperature in degrees Kelvin, and γ the ratio of specific heats at the exit plane. To preserve mass flow the radial boundary of the plume is given by

$$r = 0.5\,(D_e + z) \tag{3}$$

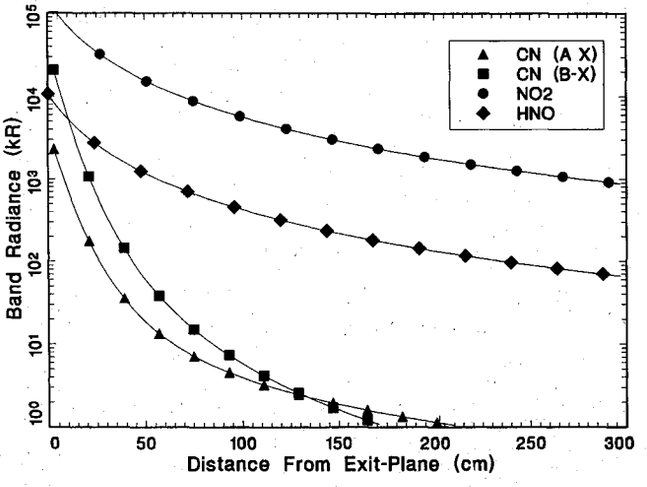

Fig. 8 Column emission rates calculated as a function of axial distance from the exit plane for the species CN (A → X), CN (B → X), NO_2, and HNO.

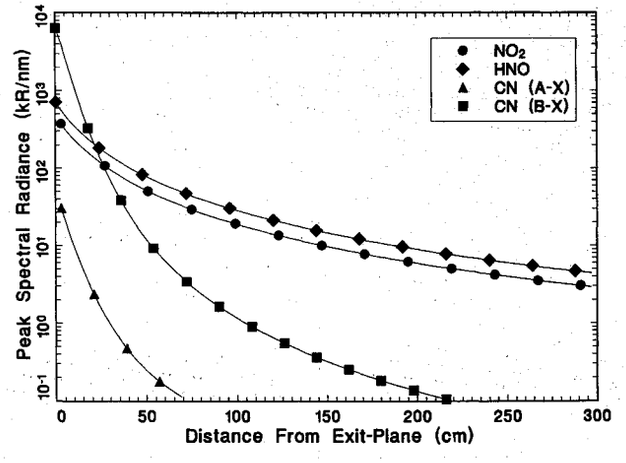

Fig. 9 Peak spectral radiance of the emissions plotted in Fig. 8 adjusted to account for the spectral resolution of the measurements.

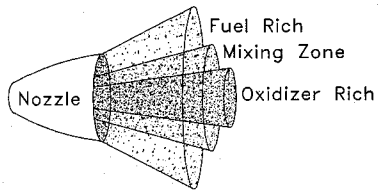

Fig. 10 Three zones of the thruster plume.

This corresponds to a conical plume with a 53-deg expansion angle. The exhaust velocity is assumed to be constant at the exit-plane value.

The plume exit-plane properties were taken from the previous PRCS analysis (summarized in Table 2). Only the mole fractions of the species that participate in the chemistry of interest here are given in Table 2. The other species are assumed to be inert. Different mole fractions are indicated for some of the species in the inner and mixing layer zones, as found in the earlier analysis. The mixing layer width is assumed to be a constant fraction of the total radial extent at each axial location. Based on earlier work, we set the fractional width of the mixing layer at 10%.

The differential equations for all of the chemical reactions in Table 3 were integrated to yield the column emission rates as a function of axial position. The results are shown in Fig. 8 for a viewing geometry that is perpendicular to and intersects the plume centerline. The results are given in terms of the total integrated band radiances and do not account for any emission that may fall outside the APE measurement spectral region (this only matters for NO_2). Another way to view the result is in terms of the peak spectral radiance for each emission band, as shown in Fig. 9. These peaks are adjusted to account for the measurement spectral resolution. The relative ordering of the features changes between Figs. 8 and 9 due to large differences in the effective spectral widths of the different emission bands. The CN emissions are negligible compared to the NO_2 and HNO emissions for axial distances beyond about 50 cm.

Discussion

The successful identification of the major features of the spectrum shown in Fig. 4 has made it possible not only to identify the emitting species (Figs. 5 and 6) but also to apply model calculations to determine the morphology of these emitting species. The spatial information requires more interpretation. As mentioned earlier, the plume can be described in terms of three regions, the fuel-rich outer region, the oxidizer-rich inner region, and the mixing zone in between (see Fig. 10). The NO_2 and HNO have similar spatial extents and, thus, are presumed to be from the same region (i.e., the inner oxidizer-rich zone). All of the other emission features in the APE data were found to arise from chemical reactions occurring in the mixing layer. Fuel-rich flows can form energetic reactive fuel fragments such as CH_2 CH, C_2 C_2O, and others by a combination of pyrolysis and oxidation chemistry. These species can then undergo very exothermic, one-step reactions with plume oxidizing species, such as O, NO, OH, and O_2, to produce electronically excited reaction products.

Acetylene (C_2H_2) plays an important role as the precursor to all of the reactive fuel fragments. In the high-temperature, fuel-rich environment, which exists near the combustor walls, C_2H_2 is a thermodynamically favored species. Equilibrium chemistry computations predict that C_2H_2 mole fractions of 0.001 or greater are plausible under these conditions. The major depletion pathway for C_2H_2, which is stable in the fuel-rich environment of the nozzle, is its reaction with atomic oxygen in the mixing layer. The resulting fragments include CH_2, CH, C_2 C_2O, and others.

Many of the reactions in the oxidation of C_2H_2 involve substantial activation energies. In the near exit-plane region, the plume is still quite hot, providing the necessary energy for these reactions to occur at significant rates. The plume temperature drops rapidly with increasing distance from the exit and as the cooling occurs, these highly endothermic reactions will cease. As a result, the emissions arising from such reactions will diminish in intensity very rapidly with distance from the exit. In particular this includes the CN(B $\rightarrow$X) violet band that has been determined to be the major uv emitter at the exit plane for a number of different motors.

By contrast, the recombination-emission reactions, which take place in the inner oxidizer-rich zone, usually do not involve an activation barrier. Often, these reactions actually increase in rate with decreasing temperature. As a consequence, the emission from these reactions can extend for a substantial distance beyond the nozzle exit. As will be quantified in the following sections, the APE measurements are entirely consistent with these expectations for emissions arising from both high and low activation barrier chemical reactions.

The reactions and associated rate constants that produce the CN, NO_2, and HNO emissions observed in the APE measurements are summarized in Table 3. This reaction set is a subset of the larger compilation used in the earlier PRCS exit-plane analysis. This subset was chosen to be a simplified, yet reasonable, representation of the most important production and depletion paths leading to the CN emission.

The initial reaction step leading to CN radiation is the abstraction of an H atom from C_2H_2 to produce the reactive fragment C_2H,

$$C_2H_2 + H \rightarrow C_2H + H_2 \qquad \text{(R1)}$$

The reverse reaction, R2, is important because of the large concentration of H_2 in the exhaust plume. Formation of the immediate CN emission precursor, C_2, proceeds directly from C_2H by three principal paths,

$$C_2H + H \rightarrow C_2 + H_2 \qquad \text{(R3)}$$

$$C_2H + OH \rightarrow C_2 + H_2O \qquad \text{(R4)}$$

and

$$C_2H + C_2H \rightarrow C_2 + C_2H_2 \qquad \text{(R5)}$$

All of the paths leading to production of C_2 [Reactions (R1) and (R3–R5)] involve at least one reaction with a substantial activation energy. The final reaction leading to CN emission had been quantitatively investigated in the laboratory[12] and was found to produce both CN(B-X) violet and CN(A-X) red band emission,

$$C_2 + NO \rightarrow CN(B) + CO \qquad \text{(R7)}$$

and

$$C_2 + NO \rightarrow CN(A) + CO \qquad \text{(R10)}$$

The branching into the CN(A) state was found to be a factor of seven times greater than for the CN(B). However, the CN(B) emission is usually the dominant spectral feature. There are two reasons for this: 1) CN(A) is more readily quenched due to its approximately two order-of-magnitude larger radiative lifetime, and 2) the CN(A) emission is distributed over a broad spectral region, whereas the CN(B) emission is confined to one dominant band feature. The Einstein *A* coefficients and plume-composition-averaged quenching rate constants for both the CN(B) and CN(A) states are indicated in Table 3. For completeness, a competitive depletion channel for C_2H has also been included in Reaction (R5).

The reaction producing NO_2 emission (R12) has been extensively investigated. It is found to proceed by way of an effective two body process for pressures as low as 10^{-4} atm. This two body process for the NO_2 and the HNO emission [Reaction (R14)] is expected to be valid over the range of plume pressures sampled in the APE measurements. The rate constant indicated in Table 3 for the NO_2 reaction has been adjusted for the effect of third body efficiencies reflecting the plume composition.

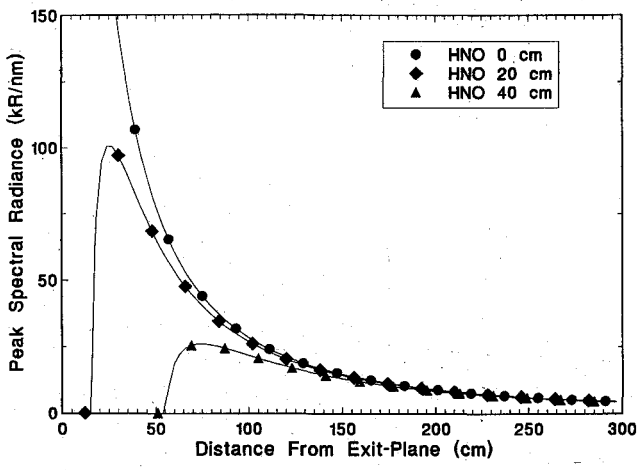

Fig. 11 Radial distribution of HNO as modified by displacement of the observing region from the centerline of the plume.

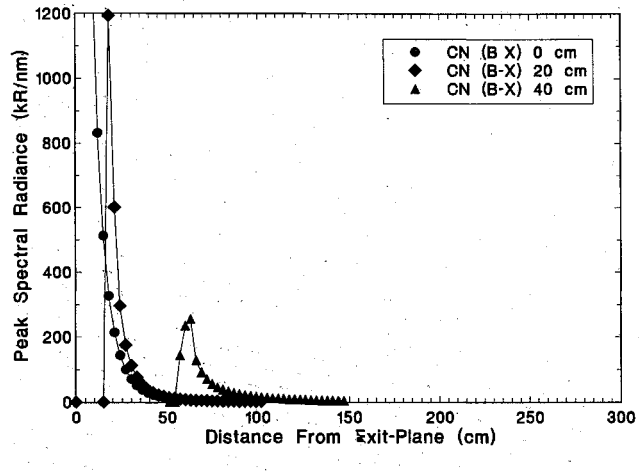

Fig. 12 Similar to Fig. 11 for the CN (B → X) emission.

The rate constant for HNO emission has not been previously measured in the laboratory. We have estimated the rate constant based on recent observations of HNO emission in ground-based exit-plane observation of the Shuttle orbital maneuvering system motor. This estimate is considered to be no better than a factor of two in accuracy.

The spatial variations of the observed emissions shown in Fig. 6 appear quite different from the predictions shown in Figs. 8 and 9. In particular, the NO_2 and HNO emissions display a local maximum at some considerable distance from the exit plane, which is not mirrored in the predictions. There is no obvious chemical mechanism or flowfield modification that can account for this behavior. It appears to arise from measurement geometry considerations, related to the difficulty in overlaying the measurement spatial footprint precisely along the plume centerline. A small parallel displacement from perfect alignment can account for most of the discrepancies between the model predictions and the data. This is demonstrated in Fig. 11 for HNO and Fig. 12 for CN where the predicted axial emission profiles as a function of the parallel displacement distance between the instrument spatial axis and the plume centerline are displayed. For HNO (NO_2 will behave similarly), the basic appearance of the data is reproduced for a displacement of about 30–40 cm. The calculations shown in Figs. 11 and 12 are similar to the data shown in Fig. 6. Exact reproduction of the observations is not expected due to the simplifications in the flowfield model. The actual plume flowfield does not have a top hat radial profile. It extends to larger expansion angles and falls off more rapidly with radial distance. This will lead to a more gradual turn on of the HNO emission. It will also push the peak to longer axial distance for a given displacement and broaden the apparent width of the feature.

The predicted CN emission shows a substantial limb-brightening effect because the emission occurs in the outer shell of the plume. A displacement of 40 cm also seems reasonable for the CN radiation. The observed spatial width of the CN emission is much larger than the predicted width. This is partly related to the simplified plume model. Some of the broadening of the features in the data may be related to the instrument spatial blur function. Although the spatial blur has not yet been fully characterized, it is estimated from the blur of star images to be about 10 cm full width half maximum. This accounts for some of the discrepancy between the predicted and observed widths.

Summary

The data presented in this report show the spatial and spectral characteristics of the near-field Shuttle-engine plume. The species HNO is identified as a major emitter in the visible. Spatial extents of CN, CH, C_2 HNO, and NO_2 are observable in the data.

Model calculations are able to explain the major emitters and their relative brightnesses. A simple extension of the exit-plane model provides insight to the spatial extent of the emitting species. Of the major emitting species mentioned, CN and CH emissions are limited to the fuel-rich zone near the exit plane. Calculations show that the brightness of these two emitters falls by more than an order of magnitude in the first 100 cm of the plume. The HNO and NO_2 emissions occur in the oxidizer-rich zone and the emissions from these species extend to the edge of the field of view of our instrument more than 300 cm from the exit plane. Discrepancies in the spatial distribution of some of the emitters can be explained by applying a simple offset from the centerline of the plume.

Further flights of this experiment are planned so that high spectral resolution and more extensive spatial information can be obtained.

Acknowledgments

The authors would like to thank W. Dimpfl (Aerospace) for suggesting that HNO emissions could be important in the visible spectral region, R. Dressler (Phillips Laboratory) for calculating the synthetic spectrum of HNO, M. Gersh (Spectral Science Inc.) for numerous discussions of plume phenomena, and astronauts F. Culbertson and R. Springer (NASA Johnson Space Center) for acquiring the data.

References

[1]Murad, E., Knecht, D. J., Viereck, R. A., Pike, C. P., Cooke, D. C., Kofsky, I. L., Trowbridge, C. A., Rall, G., Ashely, D. L. A., Twist, L., Elgin, J. B., Setayesh, A., Stair, A. T., Jr., and Blaha, J. E., "Visible Light Emission Excited by Interaction of Space Shuttle Exhaust with the Atmosphere," *Geophysical Research Letters*, Vol. 17, Nov. 1990, pp. 2205–2207.

[2]Viereck, R. A., Mende, S. B., Bernstein, L. S., Murad, E., Swenson, G. R., and Pike, C. P., "Visible Spectra of PRCS Thruster Plumes," *Proceedings of the 1992 IRIS Targets, Backgrounds and Discrimination Meeting*, Infrared Information Analysis Center, Vol. 1, Jan. 1992, pp. 79–90.

[3]Delon, R. L., "Ultraviolet Plume Measurements on the Marquardt R-40 Engine," Calspan Inc., Calspan Rept. 7458-6, Philadelphia, PA, March 1991.

[4]Bernstein, L. S., Crow, D. R., Freeman, G. N., Cox, J. W., and Lurie, J. B., "Modeling and Analysis of the Ultraviolet Emissions from the Marquardt R-40 Chamber Measurements," *Proceedings of the 1992 IRIS Targets, Backgrounds, and Discrimination Meeting*, Infrared Information Analysis Center, Vol. 1, Jan. 1992, pp. 21–47

[5]Gaydon, A. G., and Wolflhard, H. G., *Flames*, 2nd ed., rev., Chapman and Hall, London, England, UK, 1960.

[6]Becker, K. H., and Bayes, K. D., "CO Chemiluminescence from Flames," *Journal of Chemical Physics*, Vol. 48, Nov. 1968, pp. 653–661.

[7]Kydd, P. H., and Foss, W. I., "Vacuum Ultraviolet Light Emission from Low-Pressure Hydrocarbon-Oxygen Flames," *Proceedings of the Symposium on Combustion*, Vol. 11, London, 1967, pp. 1167–1182.

[8]Viereck, R. A., Mende, S. B., Murad, E., Pike, C. P., Swenson, G. R., Culbertson, F. L., and Springer, R. C., "Spectral Characteristics of the Shut-

tle Glow," *Geophysical Research Letters,* Vol. 17, May 1992, pp. 2205–2208.

[9]Bradburn, G. R., and Lilenfeld, H. V., "Absolute Emission Rate of the Reaction between Nitric Oxide and Atomic Oxygen," *Journal of Physical Chemistry,* Vol. 92, Feb. 1988, pp. 210–225.

[10]Ishiwata, T., Tanaka, I., and Akimoto, H., "Excitation of HNO by $O_2(^1\Delta_g)$," *Journal of Physical Chemistry,* Vol. 92, Dec. 1978, pp. 1336–1348.

[11]Broadfoot, A. L., Anderson, I. E., Sherard, P., Knecht, D. J., Viereck, R. A., Pike, C. P., Murad, E., Elgin, J. E., Bernstein, L. S., Kofsky, I. L., Rall, D. L., Blaha, J. E., and Culbertson, F. L., "Spectrographic Observations at Wavelengths Near 630 nm of the Interaction Between the Atmosphere and the Space Shuttle Exhaust," *Journal of Geophysical Research,* Vol. 97, Dec. 1992, pp. 19501–19508.

[12]Reisler, H., Mangir, M., and Wittig, C., "The Kinetics of Free Radicals Generated by IR Laser Photolysis I. Reactions of Ca(a) with NO, Vinyl Cyanide, and Ethylene," *Journal of Chemical Physics,* Vol. 71, April 1979, pp. 2109–2201.

[13]Dressler, R., private communication, Phillips Lab., Hanscom Air Force Base, MA, 1992.

Antoni K. Jakubowski
Associate Editor